J. Fluid Mech,. (1983), *vol.* 131, *pp.* 59–71
Printed in Great Britain

On weak reflection of water waves

By PHILIP L.-F. LIU AND TING-KUEI TSAY
School of Civil and Environmental Engineering, Cornell University, Ithaca, NY 14853

(Received 9 March 1982 and in revised form 10 November 1982)

The weak reflection of monochromatic water waves is studied for the cases of slowly varying water depth. A coupled system of equations for the forward-scattering (transmitted) and the backward-scattering (reflected) wavefields are derived from the mild-slope equation (Smith & Sprinks 1975). Parabolic approximation is then used to simplify the equations for the diffraction factor. An iterative numerical scheme is proposed to compute the resulting equations. The scheme converges very quickly for the cases of weak reflection. The accuracy of the present approach is shown by comparing with numerical results obtained by a hybrid finite-element formulation.

1. Introduction

Although the concept and the methodology of the parabolic approximation, first developed by Leontovitch (1944) and Fock (1946, 1960), has been employed for many years in different branches of the physical sciences, it is only recently that this approximation has been extended to the study of gravity water waves (Liu & Mei 1976; Radder 1979; Mei & Tuck 1980; Yue & Mei 1980; Lozano & Liu 1980; Tsay & Liu 1982; Berkhoff, Booy & Radder 1982). The primary advantage of the parabolic approximation is that it reduces an elliptic boundary value problem for wave scattering to a parabolic initial-value problem (Lundgren 1976); either analytical or numerical solutions can be obtained efficiently taking advantage of the almost-unidirectionality of wave propagation. This technique is especially useful for evaluating the wave environment in nearshore regions where caustics (or wave crossings) and wave breakings may exist.

One of the common assumptions of the work mentioned above is that the reflection or the backward scattering is either negligible or ignored. In this paper we relax this assumption. To obtain the parabolic system of equations for the forward- and the backward-scattering wavefields, we avoid formal perturbation procedures (see e.g. Lozano & Liu 1980) and adopt an approach based on the use of a 'splitting' matrix (Corones 1975; Tappert 1977). Since the mild-slope equation (see e.g. Smith & Sprinks 1975) is the base of the present analysis, the resulting parabolic system of equations is not restricted to long waves.

Assuming a weak coupling between forward- and backward-scattering wavefields, we introduce a numerical iterative scheme to solve the resulting system of equations. To demonstrate the accuracy and the efficiency of the scheme, examples concerning the scattering of a plane water wave by an elongated submerged island in an otherwise constant water depth are presented. Numerical results obtained from a hybrid finite-element formulation (Chen & Mei 1974; Tsay & Liu 1983) are used to compare with the present solutions. Good agreement is observed.

2. Derivation of governing equations

The propagation of periodic small-amplitude water waves over a slowly varying topography can be described by the following mild-slope equation (Berkhoff 1972; Smith & Sprinks 1975; Lozano & Meyer 1976):

$$\nabla \cdot (CC_g \nabla \eta) + k^2 CC_g \eta = 0, \tag{2.1}$$

where $\eta(x, y)$ is the free-surface displacement. $C = \omega/k$ and $C_g = \mathrm{d}\omega/\mathrm{d}k$ are the phase and the group velocities respectively, deducible from the dispersion relation

$$\omega^2 = gk \tanh kh, \tag{2.2}$$

where $h(x, y)$ is the water depth, ω the angular frequency, k the local wavenumber and g the gravitational acceleration.

We assume that the water depth is a constant h_0 everywhere except in a region D with slowly varying water depth. Incident waves propagating in the positive x-direction have a wavenumber k_0 which is associated with h_0 through the dispersion relation (2.2). We shall consider here the scattering of the incident waves by the bottom variations. Accordingly, we rewrite (2.1) as

$$\frac{\partial^2 \eta}{\partial x^2} + \frac{1}{CC_g} \frac{\partial CC_g}{\partial x} \frac{\partial \eta}{\partial x} + k_0^2 \mathrm{Q}^2 \eta = 0, \tag{2.3}$$

where Q^2 is a pseudodifferential operator

$$\mathrm{Q}^2 = \left(\frac{k}{k_0}\right)^2 + \frac{1}{k_0^2} \frac{\partial^2}{\partial y^2} + \frac{1}{k_0^2 CC_g} \frac{\partial CC_g}{\partial y} \frac{\partial}{\partial y}. \tag{2.4}$$

As incident waves enter the region with varying water depth, we assume that the complete wavefield can be split into a transmitted wavefield (forward scattering) and a reflected wavefield (backward scattering). This can be accomplished in many ways; for instance, one can use the Liouville–Green approximation (Carrier 1966; Meyer 1979). Here we follow Bremmer's method of a splitting matrix (see e.g. Corones 1975; Tappert 1977; Radder 1979). Thus we now introduce the new variables η_+ and η_- corresponding to the transmitted and the reflected wavefields respectively, i.e. $\eta_\pm \propto \mathrm{e}^{\pm \mathrm{i} k_0 x}$, such that

$$\eta = \eta_+ + \eta_-, \tag{2.5}$$

$$\frac{\partial \eta}{\partial x} = \mathrm{i} k_0 \mathrm{Q} (\eta_+ - \eta_-). \tag{2.6}$$

From (2.5) and (2.6) we obtain

$$\eta_+ = \frac{1}{2}\left(\eta - \frac{\mathrm{i}}{k_0 \mathrm{Q}} \frac{\partial \eta}{\partial x}\right), \tag{2.7}$$

$$\eta_- = \frac{1}{2}\left(\eta + \frac{\mathrm{i}}{k_0 \mathrm{Q}} \frac{\partial \eta}{\partial x}\right). \tag{2.8}$$

Differentiating (2.7) and (2.8) with respect to x and using (2.3) for $\partial^2\eta/\partial x^2$, (2.6) for $\partial\eta/\partial x$ and (2.5) for η, we obtain

$$\frac{\partial \eta_+}{\partial x} - \left[\mathrm{i} k_0 \mathrm{Q} - \frac{1}{2}\left(\frac{1}{\mathrm{Q}} \frac{\partial \mathrm{Q}}{\partial x} + \frac{1}{CC_g} \frac{\partial CC_g}{\partial x}\right)\right] \eta_+ = \frac{1}{2}\left(\frac{1}{\mathrm{Q}} \frac{\partial \mathrm{Q}}{\partial x} + \frac{1}{CC_g} \frac{\partial CC_g}{\partial x}\right) \eta_-, \tag{2.9}$$

$$\frac{\partial \eta_-}{\partial x} + \left[\mathrm{i} k_0 \mathrm{Q} + \frac{1}{2}\left(\frac{1}{\mathrm{Q}} \frac{\partial \mathrm{Q}}{\partial x} + \frac{1}{CC_g} \frac{\partial CC_g}{\partial x}\right)\right] \eta_- = \frac{1}{2}\left(\frac{1}{\mathrm{Q}} \frac{\partial \mathrm{Q}}{\partial x} + \frac{1}{CC_g} \frac{\partial CC_g}{\partial x}\right) \eta_+. \tag{2.10}$$

It is convenient to study (2.9) and (2.10) in terms of the diffraction factors

$$\xi_{\pm} = \eta_{\pm} e^{\mp ik_0 x}. \tag{2.11}$$

Substitution of (2.11) into (2.9) and (2.11) yields

$$\frac{\partial \xi_+}{\partial x} + \left[ik_0(1-Q) + \frac{1}{2}\left(\frac{1}{Q}\frac{\partial Q}{\partial x} + \frac{1}{CC_g}\frac{\partial CC_g}{\partial x}\right)\right]\xi_+ = \frac{1}{2}e^{-2ik_0 x}\left[\left(\frac{1}{Q}\frac{\partial Q}{\partial x} + \frac{1}{CC_g}\frac{\partial CC_g}{\partial x}\right)\xi_-\right], \tag{2.12}$$

$$\frac{\partial \xi_-}{\partial x} + \left[-ik_0(1-Q) + \frac{1}{2}\left(\frac{1}{Q}\frac{\partial Q}{\partial x} + \frac{1}{CC_g}\frac{\partial CC_g}{\partial x}\right)\right]\xi_- = \frac{1}{2}e^{2ik_0 x}\left[\left(\frac{1}{Q}\frac{\partial Q}{\partial x} + \frac{1}{CC_g}\frac{\partial CC_g}{\partial x}\right)\xi_+\right]. \tag{2.13}$$

In §3 we develop an iterative numerical scheme to solve (2.12) and (2.13) for three-dimensional forward- and backward-scattered wavefields by a submerged island.

3. Parabolic approximation for wave diffraction

To study the scattering problem where the predominating direction of wave propagation is known, we adopt the standard parabolic approximation for the diffracted wavefield. We anticipate that the diffraction factors $\xi_{\pm}$ vary slowly within a wavelength but faster in the direction of a wave front (y-direction) than it does along the wave ray (x-direction), so that

$$O\left(k_0\left|\frac{\partial \xi_{\pm}}{\partial x}\right|\right) = O\left(\left|\frac{\partial^2 \xi_{\pm}}{\partial y^2}\right|\right), \tag{3.1}$$

$$O(|k_0 \xi_{\pm}|) \gg O\left(\left|\frac{\partial \xi_{\pm}}{\partial y}\right|\right) \gg O\left(\left|\frac{\partial \xi_{\pm}}{\partial x}\right|\right). \tag{3.2}$$

The pseudodifferential operator Q appearing in (2.12) and (2.13) can be formally written as (see Tappert 1977)

$$Q = (1+\varepsilon+\delta+\nu)^{\frac{1}{2}} \tag{3.3}$$

where

$$\varepsilon = \left[\left(\frac{k}{k_0}\right)^2 - 1\right] \ll 1, \tag{3.4a}$$

$$\delta = \frac{1}{k_0^2 CC_g}\frac{\partial CC_g}{\partial y}\frac{\partial}{\partial y} \ll 1, \tag{3.4b}$$

$$\nu = \frac{1}{k_0^2}\frac{\partial^2}{\partial y^2} \ll 1. \tag{3.4c}$$

Equations (3.4a, b) are true owing to the mild-slope assumption, and (3.4c) is justified by the parabolic approximation. Expanding (3.3) in the Taylor series

$$Q \approx 1 + \tfrac{1}{2}(\varepsilon+\delta+\nu) - \tfrac{1}{8}(\varepsilon+\delta+\nu)^2 + \ldots$$

and substituting it into (2.12) and (2.13), we obtain the leading-order equations for (ξ_+, ξ_-):

$$P[\xi_+] = R\xi_-, \tag{3.5}$$

$$P^*[\xi_-] = R^*\xi_+, \tag{3.6}$$

where P is a differential operator,

$$P = \frac{i}{k_0}\frac{\partial}{\partial x} + \frac{1}{2}\left\{\left(\frac{k}{k_0}\right)^2 - 1 + \frac{i}{k_0}\left[\frac{k}{k_0}\frac{\partial}{\partial x}\left(\frac{k}{k_0}\right) + \frac{1}{CC_g}\frac{\partial CC_g}{\partial x}\right]\right\} + \frac{1}{2k_0 k}\frac{1}{CC_g}\frac{\partial CC_g}{\partial y}\frac{\partial}{\partial y} + \frac{1}{2k_0^2}\frac{\partial^2}{\partial y^2}, \tag{3.7}$$

and R is a multiplication operator,

$$\mathrm{R} = \frac{\mathrm{i}}{2k_0}\mathrm{e}^{-2\mathrm{i}k_0 x}\left[\frac{k}{k_0}\frac{\partial}{\partial x}\left(\frac{k}{k_0}\right)+\frac{1}{CC_\mathrm{g}}\frac{\partial CC_\mathrm{g}}{\partial x}\right]. \tag{3.8}$$

In (3.6) the asterisk indicates the complex conjugate. We remark that a third-derivative term $(1/k_0)\,\partial^3/\partial x\,\partial y^2$ has been ignored in (3.5) and (3.6) owing to the parabolic approximation, i.e.

$$O\left(\frac{1}{k_0}\frac{\partial^3}{\partial x\,\partial y^2}\Big/\frac{\partial^2}{\partial y^2}\right) \ll O(1) \tag{3.9}$$

We remark here that for two-dimensional problems where $\partial/\partial y = 0$ the pseudodifferential operator can be approximated as $\mathrm{Q} = 1-\frac{1}{2}[(k/k_0)^2-1]$. The two-dimensional versions of (2.12) and (2.13) are identical with those of (3.5) and (3.6). In other words, the parabolic approximation does not upset the calculations in the region where two-dimensional feature dominates.

Equations (3.5) and (3.6) are solved numerically and iteratively by adding effects of successive reflections as follows: First we assume that the reflection wavefield can be completely ignored, i.e.

$$\xi_-^{(0)} = 0. \tag{3.10}$$

Equation (3.6) yields the leading approximation for the forward-scattering wavefield:

$$\mathrm{P}[\xi_+^{(0)}] = 0. \tag{3.11}$$

The pair $(\xi_+^{(0)}, \xi_-^{(0)})$ is the first member in the sequence of pairs $(\xi_+^{(n)}, \xi_-^{(n)})$ constructed recursively with the relations

$$\mathrm{P}^*[\xi_-^{(n)}] = \mathrm{R}^*\xi_+^{(n-1)} \quad (n \geqslant 1), \tag{3.12a}$$

$$\mathrm{P}[\xi_+^{(n)}] = \mathrm{R}\xi_-^{(n)} \quad (n \geqslant 1), \tag{3.12b}$$

with suitable initial and boundary conditions.

4. Numerical examples

In this section numerical results are presented for the scattering of a plane wave by a submerged island in an infinite domain of otherwise constant depth. The cross-sectional profiles of the submerged island are shown in figure 1. For present numerical experiments the ratio of the height of the island to the water depth is taken as $b_0/h_0 = 0.25$ and the ratio of the height to the width of the base of the transversal cross-section is $b_0/l = 0.1$. The incident wave period is also fixed such that $k_0 h_0 = 0.42$. The length w of the submerged island is twice that of the incident wavelength.

Two numerical examples are given herein. The major axis of the submerged island is either parallel to ($\theta = 0°$) or normal to ($\theta = 90°$) the direction of wave propagation (x-direction). Owing to the symmetry of the problems, only one-half of the flow field ($y \leqslant 0$) is solved. To obtain numerical solutions, the computational domain is defined as $-c \leqslant x \leqslant d$, $-M \leqslant y \leqslant 0$, which encloses one-half of the submerged island. Along the x-axis the property of symmetry requires that

$$\frac{\partial \xi_+^{(n)}}{\partial y} = \frac{\partial \xi_-^{(n)}}{\partial y} = 0 \quad (y = 0). \tag{4.13}$$

If the right side boundary $y = -M$ is located far away from the submerged island, the

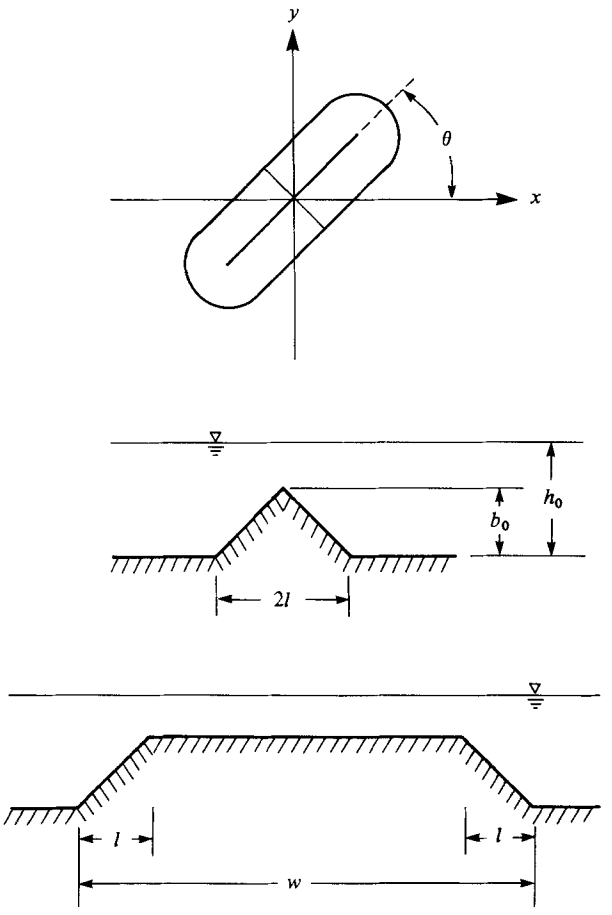

FIGURE 1. Geometrical definition of a submerged island.

magnitude of the scattered waves is small and can be ignored. Thus

$$\xi_+^{(n)} = 1 \quad (y = -M), \tag{4.14a}$$

$$\xi_-^{(n)} = 0 \quad (y = -M). \tag{4.14b}$$

Along the entrance line of the computational domain, the forward wave field is given and is normalized to be unity:

$$\xi_+^{(n)} = 1 \quad (x = -c; -M \leqslant y \leqslant 0). \tag{4.15}$$

Along the exit of the domain $x = d$, which is located in the constant-depth region, the reflected wave amplitude is zero:

$$\xi_-^{(n)} = 0 \quad (x = d; -M \leqslant y \leqslant 0). \tag{4.16}$$

Equation (3.11) is integrated from $x = -c$ to $x = d$, using (4.15) as an initial condition and (4.13) and (4.14*a*) as boundary conditions, to find $\xi_+^{(0)}$. Equation (3.12*a*) is then integrated for $\xi_-^{(n)}$ $(n = 1)$ from $x = d$ to $x = -c$, with (4.16) as an initial condition and (4.13) and (4.14*b*) as boundary conditions. Once $\xi_-^{(1)}$ is obtained everywhere inside the computational domain, (3.12*b*) can be integrated for $\xi_+^{(n)}$ $(n = 1)$ with initial condition and boundary conditions. This procedure is repeated for $n = 2, 3, 4, \ldots$ until

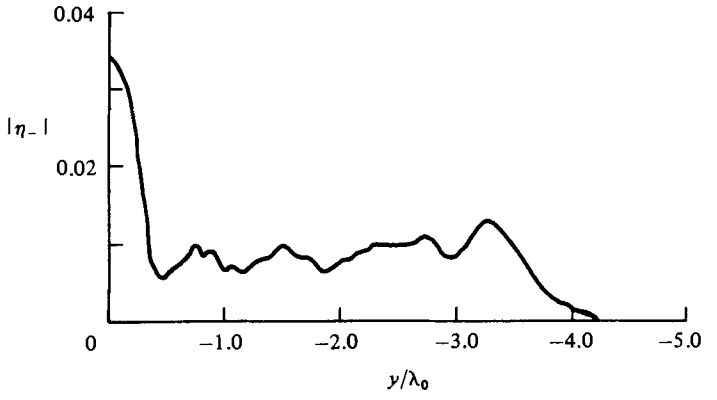

FIGURE 2. Wave amplitude of the reflected wavefield along $x/\lambda_0 = -1.0$ and $\theta = 0°$.

the converged solutions are obtained. In the present study the convergence condition is defined as

$$|\xi_{\pm}^{(n)} - \xi_{\pm}^{(n-1)}| < 10^{-4}. \tag{4.17}$$

In the numerical computations, the following data are used: $M = 5.93\lambda_0$, $c = d = 1.08\lambda_0$, where λ_0 is the incident wavelength. The entire computational domain is divided into 4,628 rectangles. Each has a dimension $\Delta x = 0.0416\lambda_0$ and $\Delta y = 0.0667\lambda_0$. The small value of $\Delta x/\lambda_0$ is required because of the factor e^{-2ik_0x} in (3.8). The Crank–Nicholson method is used to integrate (3.11) and (3.12) (for more detail see Tsay & Liu 1982). Converged solutions are obtained after two iterations ($n = 2$).

Case 1: $\theta = 0°$

For the case where the major axis of the submerged island is parallel to the x-direction, the cross-sectional area normal to the direction of wave propagation is small, $l/\lambda_0 = 0.167$. As shown in figure 2, the reflected wave amplitude $|\eta_-|$ along the line $x/\lambda_0 = -1.0$, which is in front of the submerged bank, indicates that the maximum reflection is roughly 4%. The reflected-wave amplitude drops off sharply from the centreline to the edge of the submerged island. The wave-amplitude distributions across $x/\lambda_0 = -0.5$, 0 and 0.5 are plotted in figure 3. In the same figure numerical results obtained by a hybrid finite-element method (Tsay & Liu 1983) are also shown. Agreement seems to be very good. Maximum differences occur along the centreline $y = 0$ (figure 4). Partial standing waves are observed in figure 4 owing to reflection; the distance between two adjacent crests is roughly $0.5\lambda_0$. The hybrid finite-element method (Tsay & Liu 1983) used in the computations is a direct extension of that developed by Chen & Mei (1974), which is essentially a long-wave approximation, to the mild-slope equation (2.1). The computational domain for the finite-element method is a semicircular region, enclosing the submerged island, with a radius λ_0. The semicircular domain is divided into 982 linear triangular elements with 534 nodes. The length of a typical side of a triangular element is about $0.05\lambda_0$, which is comparable to the grid size used in the present calculations. Outside of the semicircular region where the depth is constant, analytical solutions to (2.1) in a series form are used in the finite-element formulation such that the radiation boundary condition is satisfied. It should be pointed out that in the region with a constant depth, the mild-slope equation (2.1) reduces to the well-known Helmholtz equation. In numerical computations, twenty terms in the series are kept. Both the present numerical method and the finite-element method are run on the IBM 370/168 at

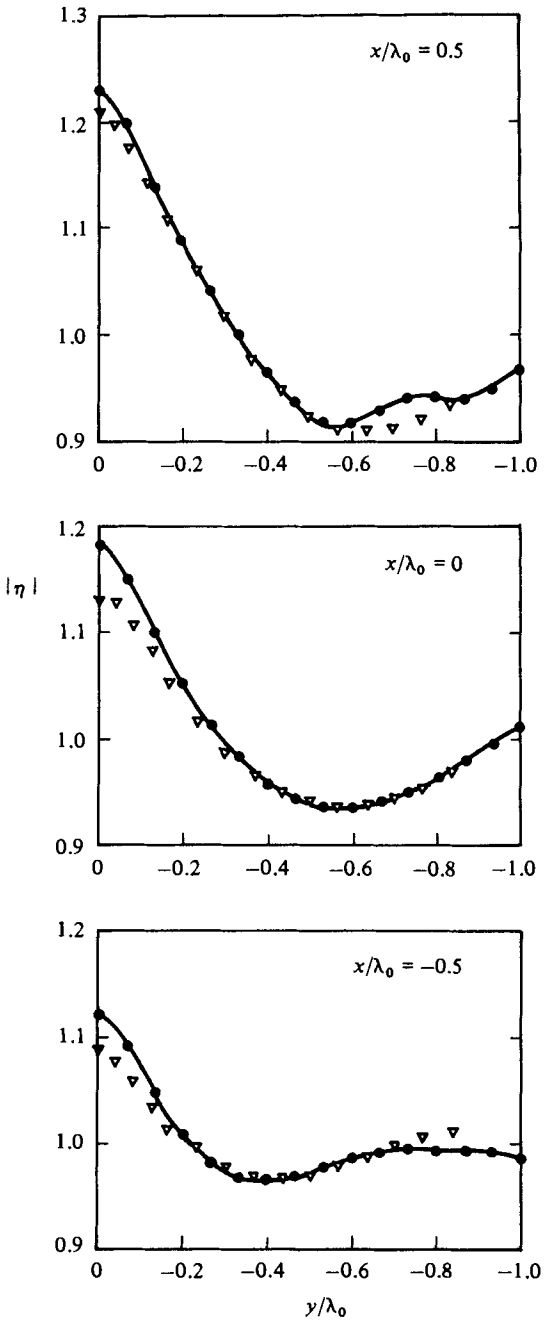

FIGURE 3. Wave-amplitude distribution of the total wavefield for $\theta = 0°$: —·—·—, present numerical results; ▽, finite element results.

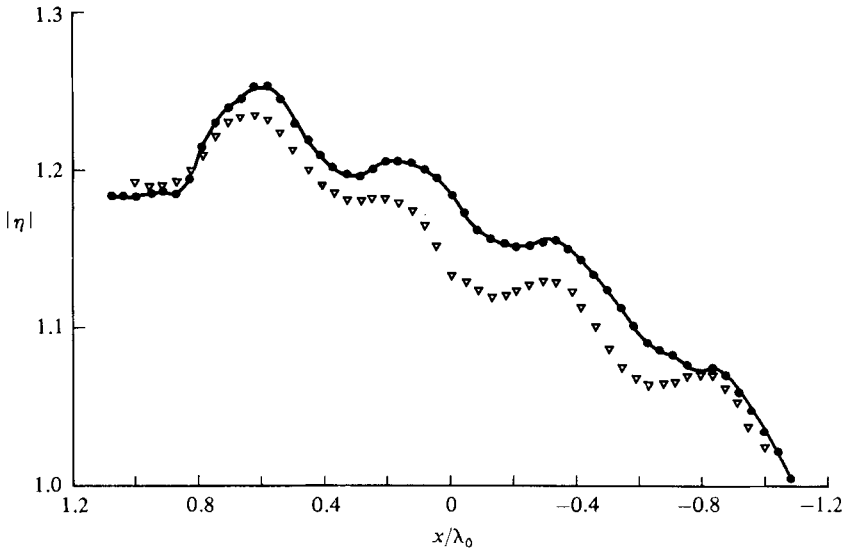

FIGURE 4. Wave-amplitude distribution along the centreline $y = 0$ for $\theta = 0°$: —·—·— present numerical results; ▽▽▽, finite-element results.

	Computer storage	CPU time	Total unknowns
Hybrid finite-element method	298K	25 s	534
Present method	210K	19 s	4770

TABLE 1. Numerical information

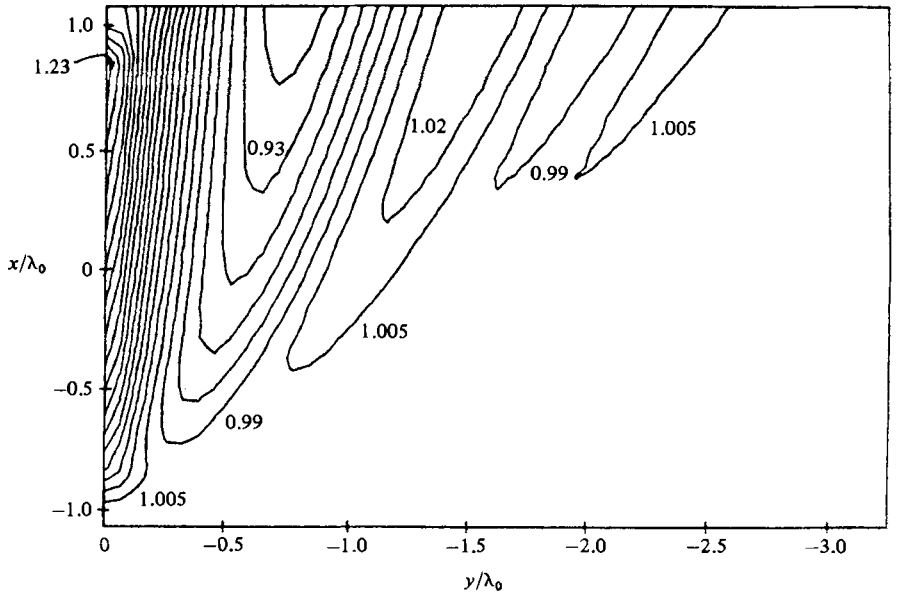

FIGURE 5. Wave-amplitude contours for the forward-scattering wavefield $|\eta_+^{(0)}|$; $\theta = 0°$.

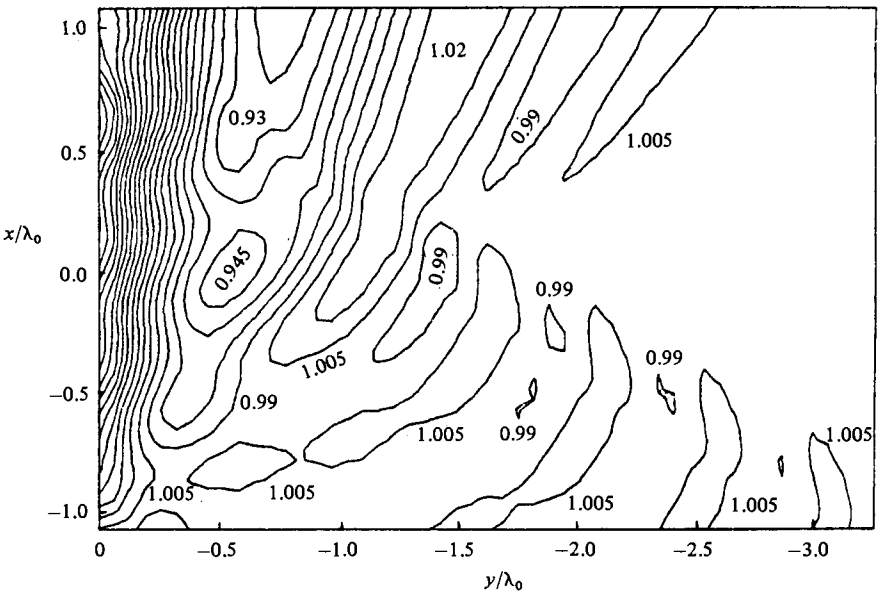

FIGURE 6. Wave-amplitude contours for the total wavefield $|\eta|$; $\theta = 0°$.

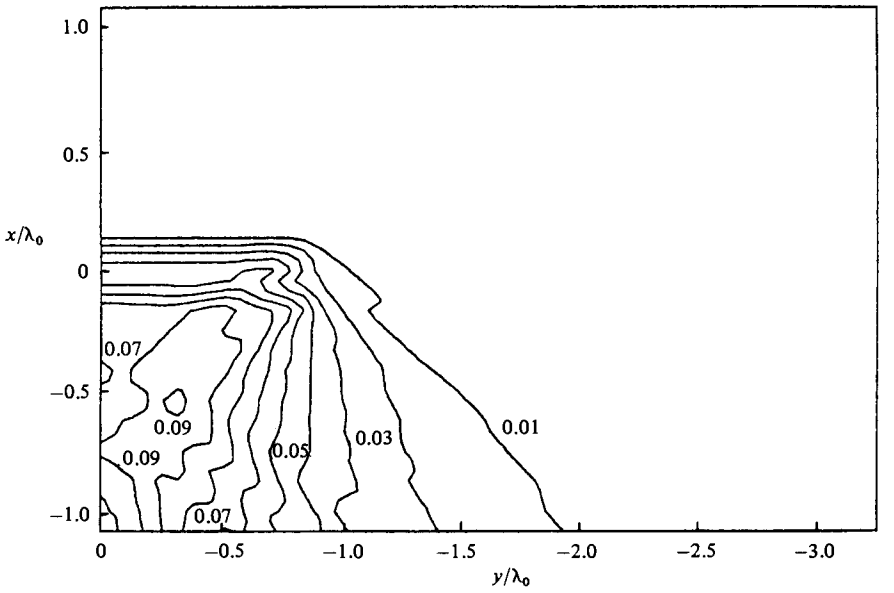

FIGURE 7. Wave-amplitude contours for the backward-scattering wavefield $|\eta_-|$; $\theta = 90°$.

Cornell University. Some of the performances and requirements by both methods are listed in table 1. It seems that the present method enjoys some advantages in both computer storage requirement and CPU time. The huge number of unknowns in the present method is due to the fact that both forward and backward wavefields $\xi_\pm$ must be stored for iterations. It is remarked here that the hybrid finite-element method is restricted to the boundary value problems where a constant water depth must appear in the far field.

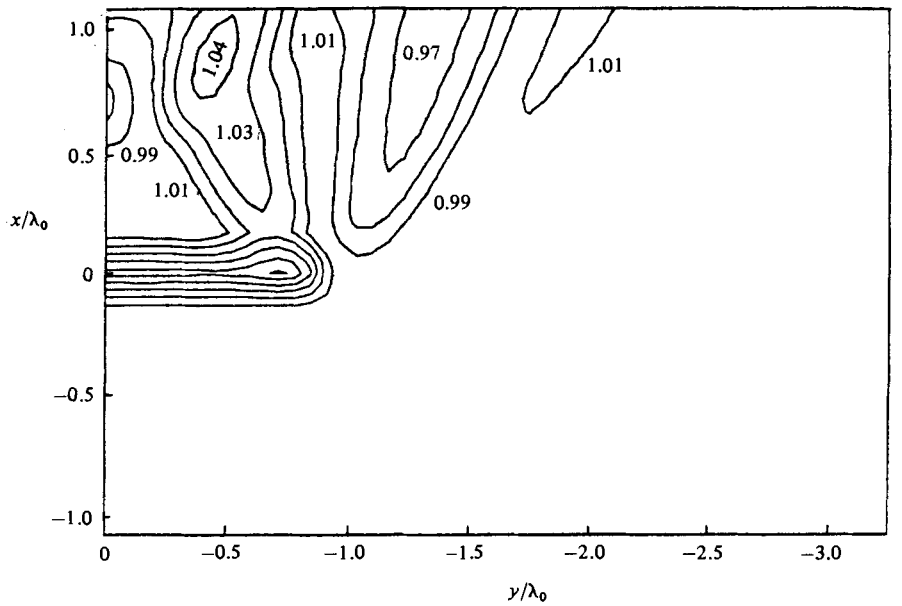

FIGURE 8. Wave-amplitude contours for the forward-scattering wavefield $|\eta_+|$; $\theta = 90°$.

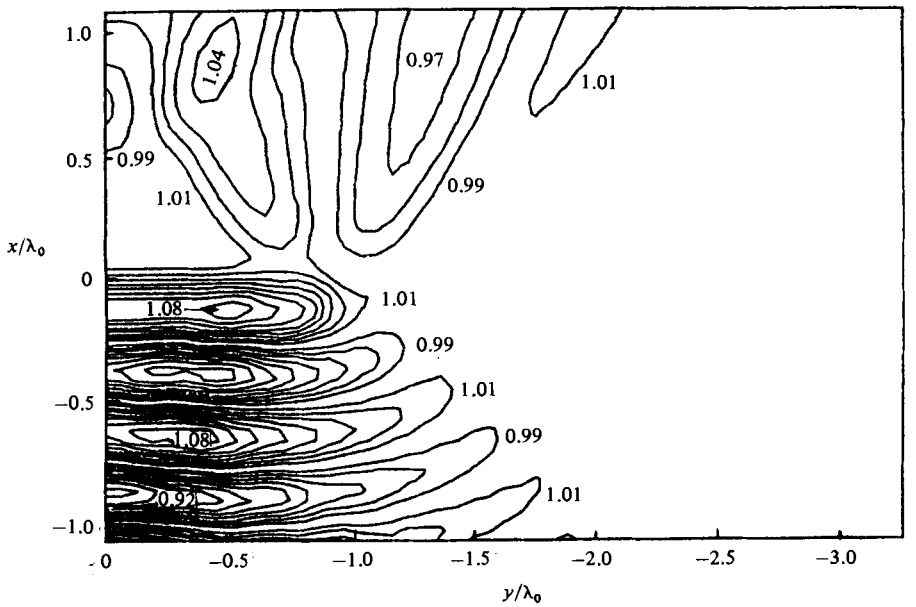

FIGURE 9. Wave-amplitude contours for the total wavefield $|\eta|$; $\theta = 90°$.

Although the total reflection is quite small in this case, the influence of reflection on the overall wave pattern can be clearly seen in figures 5 and 6. Figure 5 shows the contours of constant wave amplitudes when the reflection is entirely ignored; the forward wave field $|\xi_+^{(0)}|$ represents the situation. On the other hand, the contour lines of the wave amplitudes obtained from the converged solutions $|\eta|$ are plotted in figure 6. The increment of the contours in both figures is 0.015.

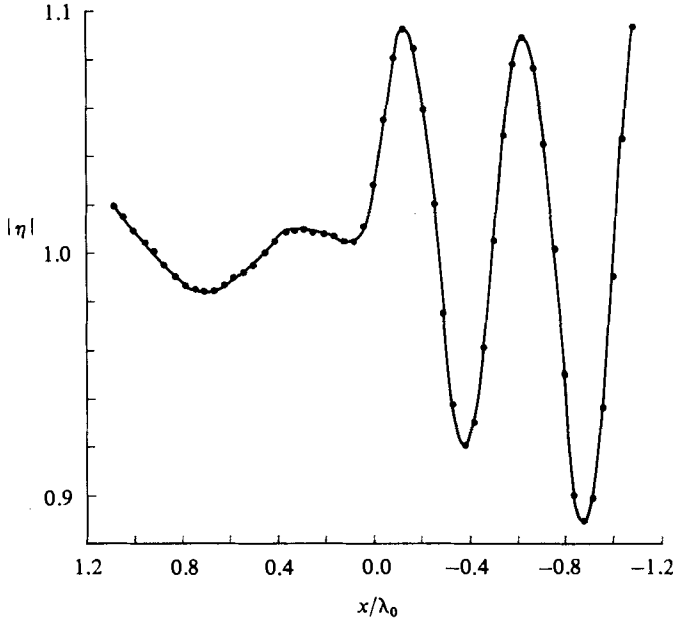

FIGURE 10. Wave-amplitude distribution along the centreline $y = 0$ for $\theta = 90°$.

Case 2: $\theta = 90°$

In the second example the direction of incident-wave propagation is perpendicular to the major axis of the submerged island. The submerged island acts as an offshore thin breakwater with high porosity, which reflects only a small portion of the incident-wave energy. Owing to the elongated shape, wave-fields over the submerged island and far away from the island are expected to be two-dimensional. The diffraction factor $\xi_{\pm}$, which is caused more or less by the tip of the submerged island, satisfies the parabolic approximation as in the case of a breakwater. In numerical computations, the same grid mesh designed for the previous example is also employed here. Converged solutions are obtained after two iterations ($n = 2$). In figures 7, 8 and 9 the contours of reflected-wave amplitudes $|\eta_-|$, transmitted wave amplitudes $|\eta_+|$ and the total wave amplitude $|\eta|$ are shown respectively. The increment of contours is 0.01. The parabolic features are clearly displaced in both forward- and backward-scattered wave fields. In figure 9, standing wave patterns are seen in front of the submerged island. The maximum reflection coefficient is approximately 10% in the present case. The wave amplitudes along the centreline $y = 0$ are also shown in figure 10. In figure 11, the total wave amplitude profiles along cross-sections $x/\lambda_0 = 1.0, 0.5, 0.0, -0.5$ and -1.0 are shown. We point out that along the major axis of the submerged island $x/\lambda_0 = 0$, the amplitude changes rather abruptly near the tip of the island. This step-function-like disturbance is then diffracted (diffused) into both forward and backward wavefields.

This research was supported, in part, by the National Sea Grant Program through a research grant to Cornell University. One of us (P. L.-F. Liu) would also like to acknowledge the financial support from the J. S. Guggenheim Foundation through a Fellowship during the course of research. Dr C. J. Lozano participated and contributed to the early stage of the research project. Referee's comments are also appreciated.

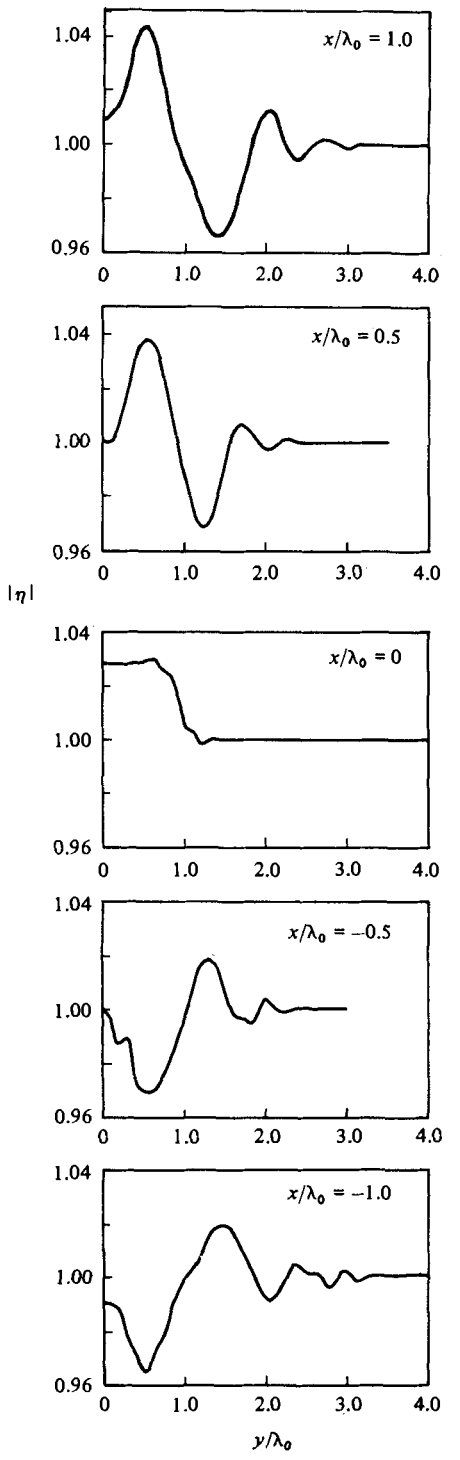

FIGURE 11. Wave-amplitude distribution along several different x-cross-sections for $\theta = 90°$.

REFERENCES

BERKHOFF, J. C. W. 1972 Computation of combined refraction-diffraction. In *Proc. 13th Coastal Engng Conf.*, vol. 2, pp. 471–490. ASCE.

BERKHOFF, J. C. W., BOOY, N. & RADDER, A. C. 1982 Verification of numerical wave propagation models for simple harmonic linear waves. *Coastal Engng* **6**, 255–279.

CARRIER, G. F. 1966 Gravity waves on water of variable depth. *J. Fluid Mech.* **24**, 641–659.

CHEN, H. S. & MEI, C. C. 1974 Oscillations and wave forces in an offshore harbor. *Tech. Rep.* no. 190, *Ralph M. Parsons Lab. for Water Resources and Hydrodynamics, Dept Civil Engng*, M.I.T.

CORONES, J. 1975 Bremmer series that correct parabolic approximations. *J. Math. Anal. Applics* **50**, 361–372.

FOCK, V. A. 1946 The field of a plane wave near the surface of a conducting body. *J. Phys. U.S.S.R.* **10**, 399–409.

FOCK, V. A., 1960 *Electromagnetic Diffraction and Propagation Problems.* Macmillan.

LEONTOVITCH, M. A. 1944 A method of solution of problems of electromagnetic wave propagation along the earth's surface. *Izv. Akad. Nauk S.S.S.R.* **8**, 16–22.

LIU, P. L.-F. & MEI, C. C. 1976 Water motion on a beach in the presence of a breakwater: 1. Waves. *J. Geophys. Res.* **81**, 3079–3084.

LOZANO, C. J. & LIU, P. L.-F. 1980 Refraction–diffraction model for linear surface gravity waves. *J. Fluid Mech.* **101**, 705–720.

LOZANO, C. J. & MEYER, R. D. 1976 Leakage and response of waves trapped by round islands. *Phys. Fluids* **19**, 1075–1088.

LUNDGREN, H. 1976 Physics and mathematics of waves in coastal zones. In *Proc. 15th Coastal Engng Conf., Hawaii*, pp. 880–885. ASCE.

MEI, C. C. & TUCK, E. O. 1980 Forward scattering by long thin bodies. *SIAM J. Appl. Maths* **39**, 178–191.

MEYER, R. E. 1979 Surface wave reflection by underwater ridges. *J. Phys. Oceanogr.* **9**, 150–157.

RADDER, A. C. 1979 On the parabolic equation method for water-wave propagation. *J. Fluid Mech.* **95**, 159–176.

SMITH, R. & SPRINKS, T. 1975 Scattering of surface waves by a conical island. *J. Fluid Mech.* **72**, 373–384.

TAPPERT, F. D. 1977 The parabolic approximation method. In *Wave Propagation and Underwater Acoustics* (ed. J. B. Keller & J. S. Papadakis), chap. V. Springer.

TSAY, T.-K. & LIU, P. L.-F. 1982 Numerical solution of water-wave refraction and diffraction problems in the parabolic approximation. *J. Geophys. Res.* **87**, 7932–7940.

TSAY, T.-K. & LIU, P. L.-F. 1983 A finite element model for wave refraction and diffraction. *J. Appl. Ocean Res.* **5**, 30–37.

YUE, D. K. P. & MEI, C. C. 1980 Forward diffraction of Stokes waves by a thin wedge. *J. Fluid Mech.* **97**, 33–52.